

# The roAp star $\alpha$ Cir as seen by BRITE-Constellation<sup>★</sup>

W. W. Weiss<sup>1 †</sup>, H.-E. Fröhlich<sup>2</sup>, A. Pigulski<sup>3 †</sup>, A. Popowicz<sup>4 †</sup>, D. Huber<sup>8</sup>, R. Kuschnig<sup>1 †</sup>, A. F. J. Moffat<sup>5 †</sup>, J. M. Matthews<sup>6 †</sup>, H. Saio<sup>10</sup>, A. Schwarzenberg-Czerny<sup>11 †</sup>, C. C. Grant<sup>7</sup>, O. Koudelka<sup>9 †</sup>, T. Lüftinger<sup>1</sup>, S. M. Rucinski<sup>12 †</sup>, G. A. Wade<sup>15 †</sup>, J. Alves<sup>1 †</sup>, M. Guedel<sup>1 †</sup>, G. Handler<sup>11 †</sup>, St. Mochnacki<sup>12 †</sup>, P. Orleanski<sup>13 †</sup>, B. Pablo<sup>5</sup>, A. Pamyatnykh<sup>11 †</sup>, T. Ramiamananantsoa<sup>5</sup>, J. Rowe<sup>14</sup>, G. Whittaker<sup>7</sup>, T. Zawistowski<sup>13</sup>, E. Zocłńska<sup>11</sup>, and K. Zwintz<sup>16 †</sup>

<sup>1</sup> University of Vienna, Institute for Astrophysics, Vienna, Austria; e-mail: werner.weiss@univie.ac.at

<sup>2</sup> Kleine Strasse 9, D-14482 Potsdam; Leibniz-Institut für Astrophysik (AIP), Potsdam, Germany; e-mail: hefrohlich@aip.de

<sup>3</sup> Astronomical Institute, University of Wrocław, Poland; e-mail: pigulski@astro.uni.wroc.pl

<sup>4</sup> Institute of Automatic Control, Silesian University of Technology, Gliwice, Poland;

<sup>5</sup> Dept. de physique, Université de Montréal;

<sup>6</sup> Dept. of Physics and Astronomy, University of British Columbia, Canada;

<sup>7</sup> Space Flight Laboratory, University of Toronto;

<sup>8</sup> Sydney Institute for Astronomy, University of Sydney, NSW 2006, Australia; SETI Institute, Mountain View, CA 94043, USA; Stellar Astrophysics Centre, Aarhus University, Aarhus C, Denmark

<sup>9</sup> Graz University of Technology, Austria;

<sup>10</sup> Astronomical Institute, Graduate School of Science, Tohoku University, Sendai, Japan;

<sup>11</sup> Nicolaus Copernicus Astronomical Center, Warsaw, Poland;

<sup>12</sup> Dept. of Astronomy and Astrophysics, University of Toronto, Canada;

<sup>13</sup> Space Research Center, Warsaw, Poland;

<sup>14</sup> NASA Ames Research Center;

<sup>15</sup> Dept. of Physics, Royal Military College of Canada, Ontario, Canada;

<sup>16</sup> Institute for Astro- and Particle Physics, University of Innsbruck;

Received / Accepted

## ABSTRACT

We report on an analysis of high-precision, multi-colour photometric observations of the rapidly-oscillating Ap (roAp) star  $\alpha$  Cir. These observations were obtained with the BRITE-CONSTELLATION, which is a coordinated mission of five nanosatellites that collects continuous millimagnitude-precision photometry of dozens of bright stars for up to 180 days at a time in two colours ( $\approx$  Johnson B and R). stands for BRiGht Target Explorer. The object  $\alpha$  Cir is the brightest roAp star and an ideal target for such investigations, facilitating the determination of oscillation frequencies with high resolution. This star is bright enough for complementary interferometry and time-resolved spectroscopy. Four satellites observed  $\alpha$  Cir for 146 d or 33 rotational cycles. Phasing the photometry according to the 4.4790 d rotational period reveals qualitatively different light variations in the two photometric bands. The phased red-band photometry is in good agreement with previously-published WIRE data, showing a light curve symmetric about phase 0.5 with a strong contribution from the first harmonic. The phased blue-band data, in contrast, show an essentially sinusoidal variation. We model both light curves with Bayesian Photometric Imaging, which suggests the presence of two large-scale, photometrically bright (relative to the surrounding photosphere) spots. We also examine the high-frequency pulsation spectrum as encoded in the photometry. Our analysis establishes the stability of the main pulsation frequency over the last  $\approx$  20 years, confirms the presence of frequency  $f_1$ , which was not detected (or the mode not excited) prior to 2006, and excludes quadrupolar modes for the main pulsation frequency.

**Key words.** Asteroseismology – Stars: chemical peculiar, oscillation, rotation, spots, fundamental parameters – Stars individual:  $\alpha$  Cir (HR 5463, HD 128898)

## 1. Introduction

$\alpha$  Cir (HD 128898, HR 5463) is a binary system whose primary component is an A7VpSrCrEu star ( $V = 3.19$ ) with a K5V companion ( $V = 8.47$ ) separated by  $16''$  (Wayman 1962). (The com-

panion is faint enough and distant enough from the primary to be ignored in the following study.) The primary component of  $\alpha$  Cir was discovered as the fifth known rapidly oscillating Ap (roAp) star in 1981 by Kurtz & Cropper (1981), followed by a frequency analysis of 47 hours of high-speed, ground-based photometry (Kurtz, Allen & Cropper 1981). These authors pointed to a variation in the amplitude of the principal pulsation, which is suspected to be due to rotational modulation. Pulsation of  $\alpha$  Cir was confirmed by Schneider & Weiss (1983) and soon after, Weiss & Schneider (1984) presented the first time-resolved simultaneous multi-colour photometry of  $\alpha$  Cir in the Walraven system. The goal was pulsation mode identification (attempted

Send offprint requests to: werner.weiss@univie.ac.at

<sup>★</sup> Based on data collected by the BRITE-CONSTELLATION satellite mission, built, launched and operated thanks to support from the Austrian Aeronautics and Space Agency, the University of Vienna, the Canadian Space Agency (CSA), the Foundation for Polish Science & Technology (FNiTP MNiSW), and National Centre for Science (NCN).

<sup>†</sup> Member of the BRITE Executive Science Team (BEST).

<sup>◇</sup> Member of the Photometry Tiger Team (PHOTT).

also by Kurtz & Balona (1984)) based on frequency multiplets and amplitude changes.

The first simultaneous time-resolved photometry and spectroscopy of  $\alpha$  Cir were obtained at ESO by Schneider & Weiss (1989). This yielded only marginal evidence for radial velocity variations for two Ca I lines and the authors remarked on the very uncertain value on the rotation period for this star (ranging in the literature from one to 12 days). Five years later, Kurtz et al. (1994) provided a robust value of the rotation period ( $P \approx 4.46$  d). Another 15 years elapsed before the first light curve sampling the full rotation cycle of  $\alpha$  Cir was published based on WIRE space photometry (Bruntt et al. 2009).

The quantity and quality of data, and the sophistication of models, has improved dramatically over the subsequent years (e.g. Kurtz et al. (1994); Audard et al. (1998); Balona & Laney (2003); Kochukhov et al. (2007); and many references therein). The most complete and recent summary of our knowledge about the pulsation of  $\alpha$  Cir is presented by Bruntt et al. (2008, 2009) and of the complex atmospheric structure and spectral signatures of pulsation by Ryabchikova et al. (2007) and Kochukhov et al. (2009).

$\alpha$  Cir was included in proposals submitted in 2009 and 2010 by several authors of this paper, responding to an Announcement of Opportunity for targets to be observed by BRITE-CONSTELLATION. Proposal #05 (WW) focused on roAp stars, #19 (DH) on 50 bright stars with the most accurately known *Hipparcos* parallaxes, and #25 (TL) on the rotation of chemically peculiar stars (in particular, possible changes in rotation period).

## 2. BRITE-Constellation photometry

The BRITE-CONSTELLATION is a coordinated mission of five nanosatellites located in low Earth orbits, each hosting an optical telescope of 3 cm aperture feeding an uncooled CCD, and observing selected targets in a  $24^\circ$  field of view (Weiss et al. 2014). Each nanosat is equipped with a single filter; three have a red filter ( $\sim 620$  nm) and two have a blue filter (central wavelength  $\sim 420$  nm). The satellites have overlapping coverage of the target fields to provide two-colour, time-resolved photometry.

The detector is a KAI-11002M CCD with 11 million  $9 \times 9 \mu\text{m}$  pixels, a 14-bit A/D converter, gain of about  $3.3 \text{ e}^-/\text{ADU}$ , and a dark current of  $1 \text{ e}^-/\text{s}$  at  $+20^\circ\text{C}$ . The saturation limit of the pixels at this temperature is  $\sim 13\,000$  ADU, and the response is linear up to about  $8\,000$  ADU. The pixel size is  $27.3''$ , projected at the sky.

The five nanosats are designated  $\alpha$ -Austria (BAb), Uni (UBr),  $\alpha$ -Lem (BLb),  $\alpha$ -Hewelius (BHR), and  $\alpha$ -Toronto (BTr), where the last letter indicates the filter on board the satellite ("b" = blue, "r" = red). A sixth nanosat,  $\alpha$ -Montréal (BMb), did not detach from its launch vehicle. The nanosats Bb and UBr were launched first, followed by BLb, BTr, and BHR.

### 2.1. $\alpha$ Cir photometry

$\alpha$  Cir was one of the targets in the Centaurus field, the second long-term pointing of BRITE-CONSTELLATION after the Orion field. The early data were obtained during science commissioning of the mission, which meant interruptions in science data collection for engineering tests. Even so, significant gaps in the time series were infrequent, caused mainly by accidental spacecraft mode changes from fine-to-coarse pointing (or tumbling) with recovery times shorter than 48 hours. New nanosats joined

the Constellation during the  $\alpha$  Cir run. As a consequence of this dynamic, instructional operational environment, the  $\alpha$  Cir data set is naturally somewhat complicated.

The data cover 25 March – 8 August 2014: 146 days, corresponding to nearly 33 stellar rotational cycles (see the next Sec. 3 for details).

$\alpha$  Cir was observed in the blue by BAb for 131 days and BLb for 26 days; in the red by UBr for 145 days, and BTr for six days. The light curves consist of nearly 44 000 blue exposures and 69 000 red exposures, each of duration 1 s in both colours. The sampling time was 21.3 s, which is set by the amount of processing time needed between consecutive exposures and the maximum amount of data that could be stored on board owing to limited download capacity at the time.

$\alpha$  Cir was observed during individual orbits for 5 to 30 min, depending on target visibility, the Earth Exclusion Angle (angular distance between the illuminated limb of the Earth and the star-tracker field of view), the required warm-up period for the star trackers after reacquisition of the target, and passages of the satellites through the South Atlantic Anomaly (when higher fluxes of cosmic rays prevent useful signal from the star trackers). There were also brief interruptions of science data collection when data were being transmitted to ground stations.

The daily data transfer rate to ground stations in Europe was less than planned because of heavy interference with unidentified transmitters on the ground, which is particularly serious during the Centaurus field observations. For example, data transfer from BAb to the station in Graz, Austria, was limited to a maximum of 15 min per orbit.

### 2.2. Reduction: standard pipeline

During the commissioning of BRITE-CONSTELLATION, the particular challenges of on-orbit photometry were assessed. To develop an efficient pipeline for fast and optimum extraction of the photometry, a Photometry Tiger Team (PHOTT) was established, consisting of three groups working independently and pursuing different processing and reduction strategies.

Issues investigated included: CCD radiation defects (warm columns, hot and cold pixels), CCD temperature variations, charge-transfer inefficiencies, pixel-to-pixel sensitivity variations and intra-pixel inhomogeneities, pointing errors, complex point spread functions (PSF) varying over the  $24^\circ$  field of view and during long observing runs, identification of defective images (e.g. incomplete PSF in a sub-raster). Competing reduction methods employed PSF fitting and aperture photometry as well as various threshold criteria for elimination of bad data points (outliers), various fit-quality parameters, median vs. mean, etc. The methods will be described in detail by Popowicz et al. (in prep.).

This investigation of  $\alpha$  Cir is based on the reduction pipeline developed by PHOTT member Adam Popowicz via aperture photometry. Figure 1 illustrates the impact of two optimisation parameters on the light-curve quality. The parameters are the threshold employed for bad-pixel identification in the mean dark frame ( $T_{\text{bad}}$ ) and the aperture radius. To assess the light-curve quality, we computed the median absolute deviations (MAD) of results obtained for individual satellite orbits, as a robust measure of scatter in the presence of outliers. The final quality measure ( $Q_M$ ) is the median of MADs defined as follows:

$$Q_M = \text{median} \left\{ \frac{\text{MAD}_i}{\sqrt{N_i}} \right\}, \quad (1)$$

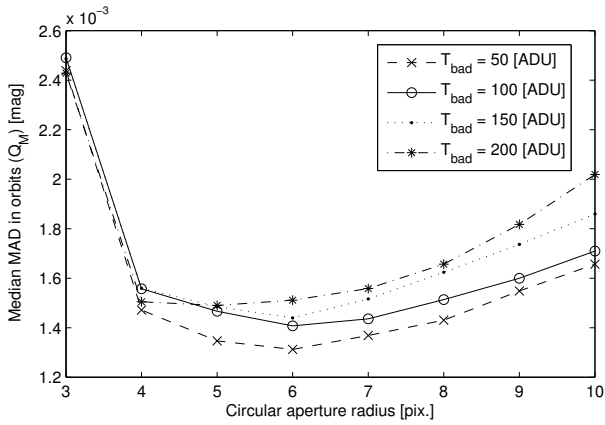


**Fig. 1.** Optimising pipeline parameters for UBr data: bad pixel elimination ( $T_{\text{bad}}$ ) and aperture radius.

where  $\text{MAD}_i$  and  $N_i$  denote the median absolute deviation and the number of measurements in the  $i$ -th orbit with a total number of orbits  $N_O$ .

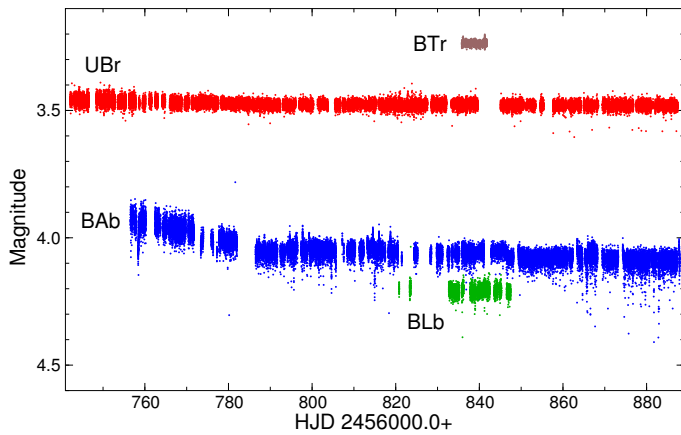


**Fig. 2.** Pipeline light curves of  $\alpha$  Cir for the four  $s$ . Note offsets for BTr and BLb and the larger scatter for the blue data.

Optimisation is the most time-consuming stage of this pipeline, so only four values for  $T_{\text{bad}}$  (50, 100, 150, and 200 ADU) and eight values for the aperture (ranging from 3 to 10 pixels) were adopted. This seems sufficient to optimise parameters for the  $\alpha$  Cir data (see minima in optimisation curves presented in Fig. 1). The final pipeline light curves from the four  $s$  that observed  $\alpha$  Cir are shown in Fig. 2.

### 2.3. Additional reductions

Figure 2 reveals that the pipeline reduction does not produce a truly clean light curve in this case, and that some outliers and instrumental effects have survived the pipeline. The pipeline data were fine-tuned in three steps: (i) removal of outliers, (ii) decorrelations, and (iii) removal of the  $s$ -satellite orbits that returned the poorest quality of photometry. (More details on fine-tuning  $s$ -pipeline-reduced data can be found in the BRITE Data Analysis Cookbook at <http://brite.craa-astro.ca/doku.php?id=cookbook>.)

First, outliers were eliminated based on a Generalized Extreme Studentized Deviate (GESD) test (Rosner 1983) applied to data obtained during a single orbit of each satellite. The number of identified outliers depends on a single parameter  $\alpha$ , increasing with larger  $\alpha$ .

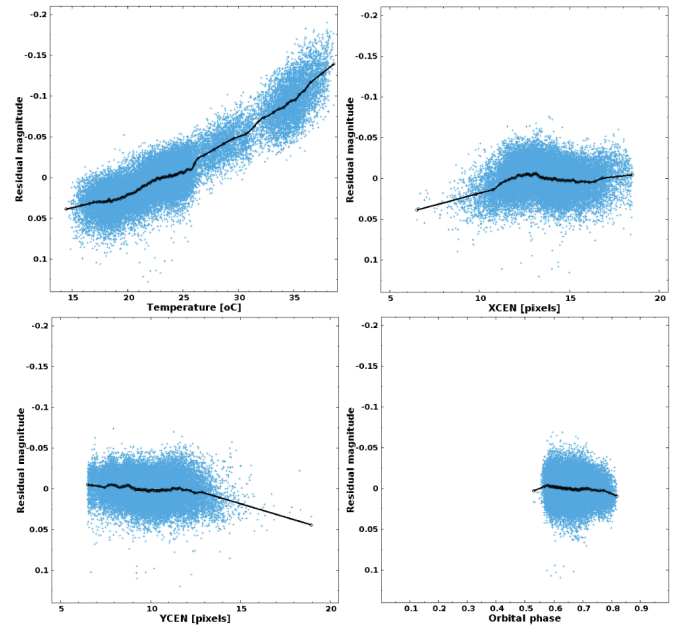


**Fig. 3.** Correlations between residual magnitudes and four instrumental parameters of BAb. The continuous line follows the Akima interpolation of bin averages.

While removing more outliers results in smaller scatter, it also results in fewer data points. Consequently, the signal detection threshold in a periodogram, which depends both on the number of data points and their scatter, can have a minimum as a function of  $\alpha$ . We adopted optimum values of  $\alpha = 0.8$  for BAb and UBr data, 0.5 for BLb, and 0.3 for BTr data, accepting a small increase in noise level. The strongest intrinsic stellar variations (the rotation frequency  $f_{\text{rot}}$ ,  $2f_{\text{rot}}$  and the main pulsation frequency near 6.5 min,  $f_1$ ) were filtered from the data prior to the outlier removal.

In the next step, we decorrelated the data with temperature, followed by a decorrelation with the position of the stellar centres in both coordinates and orbital phase, as is illustrated in Fig. 3 for BAb data. After each decorrelation, the outlier removal was repeated with the previously used  $\alpha$  parameter.

The next step towards the final light curve was rejection of the worst orbits, based on a single threshold for a given  $s$ . Although it may not be obvious in Fig. 2, there are few orbits that

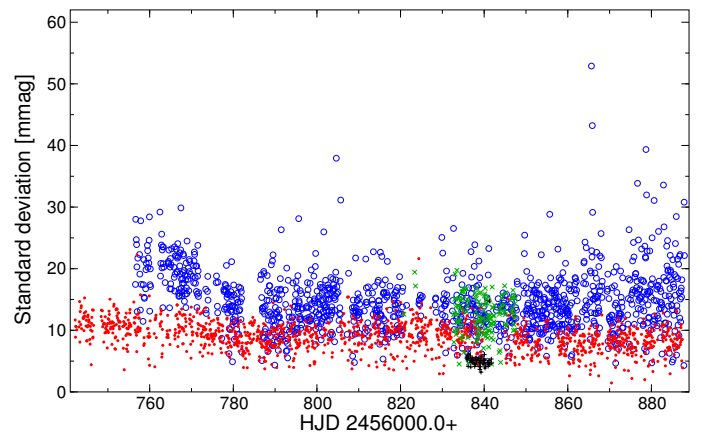


**Fig. 4.** Standard deviations for individual orbits: BAb (open circles), UBr (dots), BLb (x), BTr (+)

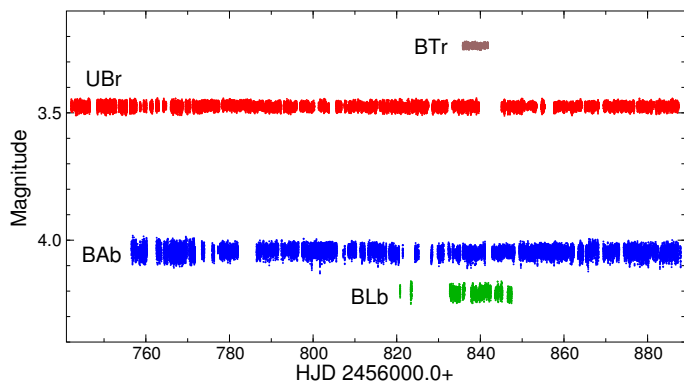


**Fig. 5.**  $\alpha$  Cir light curves after removal of the worst orbits and outliers and decorrelation. BTr and BLb data are offset for better visibility.

returned photometry of poor quality. This is better seen in Fig. 4, which shows the standard deviations in mmag for individual orbits. Based on this, the chosen thresholds are: 26 mmag for BAb, 25 mmag for BLb, 17 mmag for UBr, and 8 mmag for BTr.

Comparing Fig. 5 with Fig. 2 illustrates the improvements achieved by fine-tuning the original pipeline data. The systematic decrease of BAb magnitudes (for example, early in the observing run and seen in Fig. 2) disappeared because it was caused by CCD temperature variations (Fig. 3, upper left). After fine-tuning, a total of 61 988 red and 34 592 blue data remain.

### 3. Rotation of $\alpha$ Cir

The first indirect evidence of the rotation period of  $\alpha$  Cir was reported by Kurtz et al. (1994) who deduced a rotation period of about 4.46 days from the amplitude modulation of the star's main pulsation mode. This initial estimate was refined to 4.4790 days (Kurtz, op.cit) through photometry collected over the following 12 years from various observing campaigns.  $\alpha$  Cir was observed by the WIRE satellite star tracker for a total of 84 days during September 2000 – July 2006, supported by ground-based Johnson B photometry from SAAO. These data led to the first rotation light curve of  $\alpha$  Cir (Bruntt et al. 2009).

BRITE-CONSTELLATION takes the analysis of  $\alpha$  Cir to a new stage compared to WIRE by providing space-based photometry in two colours. The photometry is plotted in phase with the rotation period in Fig. 6. The noise level for the blue data is larger, mostly due to problems with the BAb star tracker and as a result of the spectral type, which produces a smaller count rate for the blue  $s$  compared to the red BRITEs. The rotation light curves are obviously different in the two colours. While one maximum at approximately phase  $\phi = 0.8$  appears in both filters, the second maximum in red at about  $\phi = 0.2$  is not present in blue (see Fig. 6). This difference is significant, likely indicating very peculiar spot properties and posing a challenge to interpret physically.

For comparison, we digitised Fig. 2 of Bruntt et al. (2009) and, in our Fig. 7, plotted their 100 WIRE data points from July 2006 along with our red data (similar in bandpass to the WIRE data). We conclude that the rotational modulation pattern has been stable between 2006 and 2013/14. When comparing the scatter, one should keep in mind that (1) BRITE-CONSTELLATION data are based on 1 s integrations sampled every 21 s, while WIRE data were obtained twice per second, co-added in 15 s bins; and (2) the collecting area of the WIRE star-tracker telescope is three times larger than the telescope.

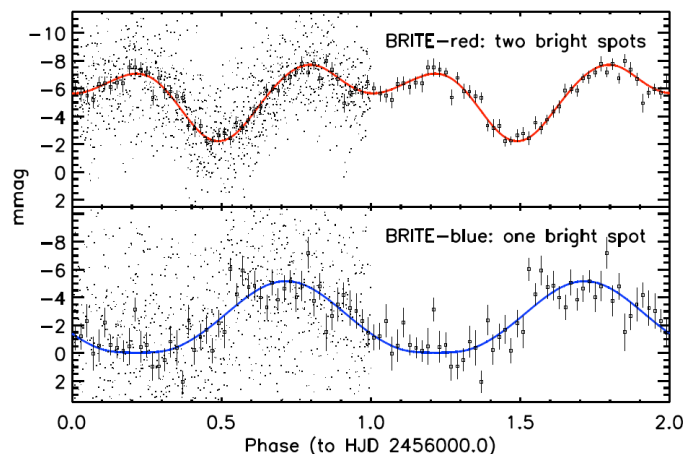


**Fig. 6.** Rotation of  $\alpha$  Cir observed by the red-sensitive (top) and blue-sensitive (bottom)  $s$ , respectively, with  $P_{rot} = 4.4790^d$ . Phase-bin averages with  $1-\sigma$  errors are given together with the theoretical light curve obtained for the respective spot model (see Sec. 4). Phases 0 to 1 also show the binned original data with an overall r.m.s. noise of 9 mmag for the red and of 15 mmag for the blue light curve.

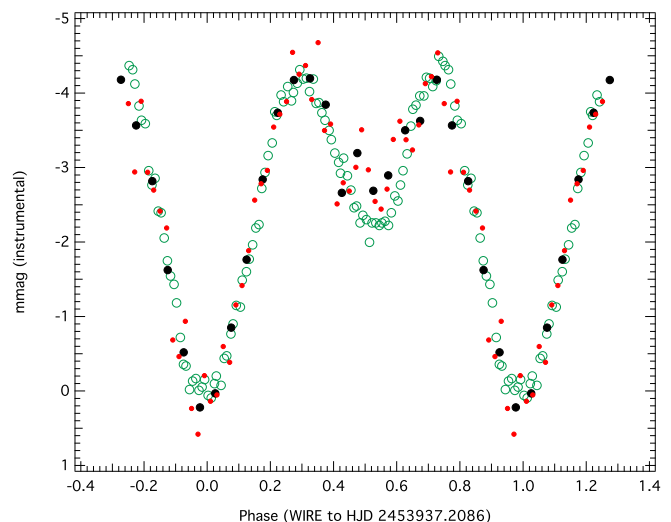


**Fig. 7.** Rotation of  $\alpha$  Cir. Green circles: WIRE - 2006 July data (Fig. 2 of Bruntt et al. (2009)). Dots: UBr and BTr data (red filter) with a phase binning of 0.01 (small red dots) and of 0.05 (large black dots). The data were scaled to fit the amplitude range of WIRE and shifted in phase to be compatible with the different reference time in HJD for WIRE and  $s$ .

### 4. Bayesian photometric imaging (BPI)

Ap stars, such as  $\alpha$  Cir, are well known to exhibit surface abundance nonuniformities (abundance spots) produced as a consequence of chemical diffusion in the presence of their strong magnetic fields. As described by, for example Krtićka et al. (2009), photometric variability of these stars is believed to result from flux redistribution principally because of variable line blanketing modulated by stellar rotation.  $\alpha$  Cir exhibits obvious photometric variability on the rotational timescale that we interpret to be indicative of such spots.



#### 4.1. Likelihood estimate

The Bayesian photometric imaging (BPI) technique to construct a spot model based on a light curve well sampled in time is described in detail by Lüftinger et al. (2010a). Below we only comment on the construction of the likelihood function, vital for any parameter estimation.

To save computation time, the fine-tuned data were combined into bins with a maximum width of 36 min. This bin width corresponds to roughly one-third of the orbital period of one *\_satellite*. The time difference between adjacent points within a bin does not exceed 15 min. With these chosen bin constraints, no bin contains fewer than ten data points. Each of the 1368 red and 1200 blue bins was assigned a weight according to the number of contributing data points within a bin and used for the BPI procedure described below.

We assume the residuals, deviations between observation and model, are Gaussian-distributed, i.e. measurement errors augmented by systematic (model) errors. To enhance robustness, the variance of the residuals was assumed to be unknown and regarded as a mere nuisance parameter. The Gaussian likelihood function was integrated by applying Jeffreys' prior (Jeffreys 1961). In our case, the improper (not normalisable) prior varies with the reciprocal of the variance. We took into account that the binned data points have different weights. This error-integrated likelihood was then integrated analytically over all possible magnitude offsets.

The resulting likelihood is a function of the data alone, given a set of parameter values. It is a comforting feature of this type of data analysis that the error variance and any magnitude offset, although they remain undetermined, can be ignored, which reduces the number of free parameters and enhances robustness.

To reduce the number of free parameters as much as possible, we took the star's inclination to be  $i = 36^\circ$ . This value results from the measured projected rotational velocity,  $v \cdot \sin(i)$ , the assumed value of the stellar radius (Bruntt et al. 2008), and the rotational period of 4.4790 days (Kurtz et al. 1994). As the limb-darkening coefficient is unknown, it was regarded as a nuisance parameter for the present study. For the high-quality WIRE data, however, in a follow-up study it might also be possible to extract the marginal distribution of the coefficient for linear limb darkening.

The outcome of a Bayesian parameter estimation is the posterior probability distribution in an high-dimensional parameter space. Direct numerical brute-force integration often requires prohibitively large computing resources, so we used the Markov chain Monte Carlo method (MCMC; cf. Press et al. (2007)). The likelihood mountain in the six-dimensional space is explored by up to 64 Markov chains. In a relaxed state, each parameter's marginal distribution is revealed by counting how often an element in parameter space is frequented by the chains.

A marginal distribution describes a parameter's probability distribution irrespective of the values of all the other parameters, i.e. disregarding correlations between parameters. These distributions are reflected in Tables 1 and 2 by presenting the corresponding credibility intervals. It is an advantage of the Bayesian approach that parameter averages, such as expectation or median as well as credibility intervals, are deduced from the measured data alone.

#### 4.2. Surface spot models

We restrict our discussion to two-spot models since the information content of the presently available *\_data* does not enable

**Table 1.** Parameters for circular spots for the *\_red*, WIRE, and *\_blue* solutions, assuming two dark spots. We list expectation values and 90% credibility limits for the central longitude ( $\lambda$ ), latitude ( $\beta$ ), and radius ( $\gamma$ ). Radii and their uncertainties are modelled for a spot intensity of 60% of the unperturbed photosphere.

Parameter	<i>_red</i>	WIRE	<i>_blue</i>
first spot			
$\lambda$	$74^\circ 3^{+2.4}_{-2.4}$	$89^\circ 4^{+0.8}_{-0.7}$	$209^\circ {}^{+24}_{-29}$
$\beta$	$-72^\circ 7^{+5.5}_{-5.2}$	$-2^\circ 8^{+3.4}_{-3.7}$	$36^\circ {}^{+41}_{-33}$
$\gamma$	$58^\circ 2^{+6.2}_{-6.3}$	$8^\circ 0^{+0.4}_{-0.3}$	$6^\circ {}^{+2}_{-2}$
second spot			
$\lambda$	$248^\circ 5^{+6.2}_{-6.2}$	$263^\circ 4^{+1.3}_{-1.3}$	$118^\circ {}^{+12}_{-14}$
$\beta$	$6^\circ 0^{+44.8}_{-30.8}$	$-18^\circ 7^{+2.9}_{-3.1}$	$-24^\circ {}^{+25}_{-35}$
$\gamma$	$6^\circ 0^{+1.8}_{-2.2}$	$8^\circ 3^{+0.7}_{-0.7}$	$16^\circ {}^{+15}_{-11}$
residuals	$\pm 2.1$	$\pm 0.14$	$\pm 4.8$

us to consider more than two spots. The WIRE data do contain more information, which we plan to explore in a future study. The main picture, however, very probably will remain the same.

In our model, two types of circular spots are allowed: dark spots with a brightness of 60% of the brightness of the undisturbed photosphere and bright spots with a brightness of 125%. The latter values are similar to what has been reported for the spots of HD 50773 by Lüftinger et al. (2010a), based, as is already mentioned, on an independent analysis of space-based photometry and ground-based Doppler imaging.

The reason for a fixed common spot brightness is the unavoidable degeneracy between spot area and spot brightness, which prevents the MCMC method to converge to a relaxed solution of the posterior probability density distribution. The data simply do not constrain both parameters independently. Hence, we had no choice but to prescribe the spot brightness parameter, but these are based on examples in the literature. As a test, we repeated the modelling with a  $\kappa$  arbitrarily set to 1.5 and expected the inferred spot size to be reduced by about 50%. Indeed, we found a factor of 1.84, which corresponds to a spot size reduced to 0.54 of the original size. Interestingly, this spot size reduction with increased kappa only holds for the spot that is fully visible. The large spot at the south pole, which basically is visible most of the time, but never entirely, is only reduced by 4% and its centre moves 6 degrees towards the pole. It is hardly necessary to stress that it would make even less sense (from the data analysing point of view) to consider spots with individual surface brightnesses. The model spot parameters must be therefore considered with reservation and taken rather as an order-of-magnitude estimate.

The following parameters were estimated for each circular spot: the central longitude ( $\lambda$ ), latitude ( $\beta$ ), and angular radius ( $\gamma$ ). The longitude increases in the direction of stellar rotation, and the zero point is the central meridian facing the observer at the beginning of the time series (HJD = 2456742.188).

Table 1 and 2 summarise what we can say about the locations and sizes of spots on the surface of  $\alpha$  Cir based on a Bayesian analysis of the red and blue *\_light* curves and the WIRE light curve. The importance parameter, justifying the attribute "first" and "second" to a spot, indicates the impact on the light curve. Listed are expectation values and 90% credibility intervals (not to be confused with  $\pm 1 \sigma$  limits).

**Table 2.** The same as Table 1, but assuming bright spots. No two-spot solution was obtained for the `_blue` data. Radii and their uncertainties are modelled for a spot intensity of 125% of the unperturbed photosphere.

Parameter	<code>_red</code>	WIRE	<code>_blue</code>
first spot			
$\lambda$	$326^{\circ}5^{+7.8}_{-7.4}$	$356^{\circ}9^{+0.9}_{-0.8}$	$356^{\circ}^{+8}_{-8}$
$\beta$	$31^{\circ}7^{+25.1}_{-21.9}$	$25^{\circ}9^{+4.3}_{-4.4}$	$34^{\circ}^{+27}_{-23}$
$\gamma$	$9^{\circ}6^{+2.0}_{-2.0}$	$13^{\circ}7^{+1.4}_{-1.4}$	$8^{\circ}^{+1}_{-1}$
second spot			
$\lambda$	$172^{\circ}2^{+7.3}_{-7.6}$	$186^{\circ}1^{+2.0}_{-2.0}$	no solution
$\beta$	$-73^{\circ}8^{+5.2}_{-5.3}$	$-82^{\circ}8^{+1.4}_{-1.5}$	
$\gamma$	$64^{\circ}2^{+7.3}_{-7.2}$	$85^{\circ}2^{+4.4}_{-3.6}$	
residuals	$\pm 2.1$	$\pm 0.13$	$\pm 4.9$

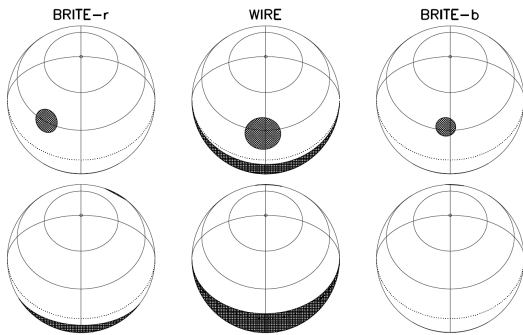


**Fig. 8.** Maps of bright spots based on `_blue`, `_red`, and WIRE according to the parameters given in Table 2. Two rotation phases shown (top and bottom) differ by  $180^{\circ}$ . The Bayesian technique cannot identify a spot at the stellar south pole with sufficient probability for the `_blue` data, probably because of a lower photometric accuracy.

A comparison of the tables shows that dark and bright spots individually fit the BRITE-CONSTELLATION and WIRE data equally well, i.e. we find similar credibility limits. The model light curves (full lines in Fig. 6) look very much the same and give the same residuals to the observations, regardless of whether the spots are dark or bright. However, important differences come to light in a detailed examination.

The surface mapping for two dark circular spots with the red `_and` WIRE data requires a separation of  $180^{\circ}$  in longitude with spots on opposite sides of the star. Two dark spots, which fit the blue `_data`, however, are separated by nearly  $90^{\circ}$  in longitude and do not agree with the red map. This suggests that bright spots are a more realistic fit to the entire data set than dark spots.

We only find a spot model that agrees with WIRE and both `_data` sets in the case of bright spots. However, only one bright spot could be detected in the `_blue` data, which is not surprising, considering the differences in the red and blue `_light` curves (see Fig. 6). A schematic of what we believe is the most realistic surface model for  $\alpha$  Cir (see Table 2) is provided in Fig. 8. The spot close to the stellar south pole is credibly present in the WIRE

and `_red` data, but not in the `_blue` data, which have the lowest precision.

An inhomogeneous surface distribution of elements, like Si, Cr, and Fe, are known to cause variations in the light curves of many Ap stars detectable as bright spots in visual photometry (e.g. Lüftinger et al. 2010a,b; Krtićka et al. 2009, 2012, 2015; Shulyak et al. 2010). This is a strong argument to favour bright spot solutions over dark spot solutions, if no other information is available. The size of abundance spots is independent of wavelength, which is what we find for the bright spot model within twice the credibility limits.

Bayesian techniques provide an infinite number of feasible two-spot solutions, but these differ in credibility. A main problem in our case is the skewness of the marginal distribution for the parameters, in particular, for the `_data`, as is evident from the asymmetric 90% credibility intervals, which is also listed in both tables. The focus of our investigation is on the expectation values of the parameters' marginal distributions. Such a spot model is, in a certain sense, the most representative, but because of the posterior's skewness, this model may differ from the globally most probable model (the 'best-fit model').

#### 4.3. Significance of BSI models

In the previous Section we tried to model the observed light curves obtained in different colours with circular areas at the stellar surface (spots), which manifest themselves to the observer as periodically varying disk averages obtained at various rotation phases. Stellar surface structures can be very complicated because they depend on temperature, gravity, dynamics in the atmosphere, element abundances, and magnetic field, all of these as a functions of optical depth. In addition, insufficient knowledge of atomic and molecular transition properties and energy level splittings in the presence of a magnetic field can have serious effects on how such surface areas are interpreted by observers.

The transformation of a one-dimensional function, the light curve, into a two-dimensional surface map obviously requires simplifying assumptions. An adjustable model constrained by disk-averaged flux measurements, obtained with three broadband filters at a discrete set of rotation phases, cannot represent the complex physics and chemistry of a stellar atmosphere, but can indicate locations of inhomogeneities. Unfortunately, in the present investigation we only have a limited amount of information available for  $\alpha$  Cir to map the complex surface. Photometric surface models cannot recover information about properties such as abundances and temperature, but they can indicate areas with inhomogeneities at the stellar surface. In addition from consistency arguments, they can indicate a preference for flux excess or depression with no reference to an underlying physics. Therefore, a realistic starting point is a model, which is as simple as possible and is tested against the observations, which in our case is light curves.

The Bayesian approach offers two attractive features: (a) the quantitative comparison of models differing in the number of spots and (b) the derivation of credibility intervals for the model parameters from the posterior probability distribution. Our two-spot model is sufficient to reproduce the photometry with the best probability distribution possible so far. Adding more features may suggest a better visual representation of the light curve, but considering the noise level of the data, increased complexity reduces the over-all credibility of the model. Indeed, we have investigated more complex models (e.g. three spots, different limb darkening coefficients, and spots of different bright-

ness), but had to accept that all these additional model features did not increase the credibility. Moreover, with too many free parameters involved, the method does not work because the Markov chains do not converge to a well-constrained posterior probability density distribution. The only remedy are additional observations that access new parameter space, such as high spectral and time-resolved spectroscopy and/or spectropolarimetry. The limited amount of presently available data, their quality and physical information content simply do not allow for a more sophisticated spot modelling, for example for disentangling  $\kappa$  and size of spots.

Nevertheless, our present model serves as a reasonable starting point for more sophisticated modelling of the surface structure, for example based on future analysis of spectroscopic and/or spectropolarimetric data. This expectation is supported by the results of Lüftinger et al. (2010a) for HD 50773, where essentially the same surface pattern was determined independently from Bayesian spot modelling of space-based photometry (CoRoT) and from Doppler imaging modelling of spectropolarimetric data. Even more significantly, Alentjev & Mkrtchian (2010) report surface abundance maps of Cr II in their preliminary Doppler imaging analysis, which support our model (= course map of inhomogeneities) derived from photometry.

## 5. Pulsation frequencies, amplitudes, and phases

The pulsation spectrum of  $\alpha$  Cir shows a dominant mode with a period of  $\sim 6.5$  min ( $f_1$ ), which is rotationally split into a triplet by rotation (Kurtz et al. 1994). Four additional low-amplitude frequencies ( $f_2$  to  $f_5$ ), attributed to roAp oscillations, were reported by Kurtz et al. (1994). Using WIRE data, Bruntt et al. (2009) confirmed two of these low-amplitude modes ( $f_4$  and  $f_5$ ), while  $f_2$  and  $f_3$  remained undetected.

Bruntt et al. (2009) also reported detection of two new frequencies ( $f_6$  and  $f_7$ ) that are symmetrical to  $f_1$ , which had not been seen in previous ground-based campaigns nor in the WIRE 2000 and 2005 data.

### 5.1. Frequencies

We first removed the contribution of rotational variability and instrumental effects ( $1d^{-1}$ ,  $2d^{-1}$ , orbital frequency and its harmonics) from the light curves with a multi-sine fit provided by Period04 (Lenz & Breger 2005). Next, we calculated amplitude spectra and estimated the statistical significance of frequencies via SigSpec (Reegen 2007, 2011), which has previously been extensively applied to space-based photometry from MOST, including roAp stars (Gruberbauer et al. 2008; Huber et al. 2008). Figure 9 shows the amplitude spectra of the red and blue data centred on the frequency range where oscillations had already been observed in  $\alpha$  Cir. The dominant mode near  $\sim 6.5$  min ( $\sim 2442 \mu\text{Hz}$ ) is clearly detected in both data sets. As expected, the amplitude is significantly higher in the blue than in the red filter.

The top panels of Fig. 10 show a close-up of  $f_1$  demonstrating that the rotationally split side lobes remain undetected in the data. This is not due to the removal of the rotational variability from the light curve, since the multiplet is caused by rotational amplitude modulation of  $f_1$  as a consequence of the oblique pulsator model (Kurtz & Shibahashi 1986). The apparent contradiction of an  $f_1$  amplitude changing with rotation period and the lack of rotation side lobes seen in the frequency spectrum of our data is due to very small amplitudes. Kurtz et al. (1994) estimated these side-lobe amplitudes to be about one-tenths of the

main amplitude ( $= 0.55$  mmag for  $f_1$  and our red  $\underline{s}$ ) and give a justification for this value within the framework of the oblique pulsator model.

The middle and bottom panels of Fig. 10 show the amplitude spectra after pre-whitening the data by the dominant mode  $f_1$  and we detect  $f_7$  in the red data, while in both data sets  $f_6$  remains below the detection threshold (S/N ratio of  $\sim 4$ ). This ratio corresponds to a significance limit of  $10^{-5.46}$ , or to a 99.9% detection probability of a true signal (Kuschnig et al. 1997). The amplitude ratios are  $A(f_1)/A(f_7) = 3.468(\pm 0.007)$  for WIRE and  $2.51(\pm 0.10)$  for red. Bruntt et al. (2009) speculate that  $f_6$  and  $f_7$  first appeared between 2005 and 2006 and interpreted them as consecutive overtones of a new pulsation mode. Unfortunately, the noise level of the blue data does not enable a detection of  $f_7$ , which would be helpful in discussing the pulsation mode. It has to be proven by follow-up observations that indeed a mode that is different in parity than  $f_1$  has been excited. A new mode of the same parity would have produced a frequency separation that is twice as large (see discussion in Bruntt et al. (2009)).

Using the frequencies identified with SigSpec, we applied Period04 (Lenz & Breger 2005) to calculate least-squares fits for frequency, amplitude, and phase to each light curve. For  $f_1$  we fixed the frequency to the best-fit values from the blue data, which has higher significance than the red data. Uncertainties on all values were calculated with Monte Carlo simulations, which are implemented in Period04. The final values, uncertainties, and significances are listed in Table 3.

### 5.2. Amplitudes and phases

The pulsation amplitude ratio for  $f_1$  measured from observations is  $A_B/A_R = 3.15 \pm 0.33$ , compared to  $A_B/A_{WIRE} = 2.32 \pm 0.11$  by Bruntt et al. (2009) and  $A_B/A_V = 2.28 \pm 0.26$  by Kurtz & Balona (1984). Formally, all values agree within  $2\sigma$ , and the amplitude ratio seems to confirm the conclusion by Bruntt et al. (2009) that the WIRE bandpass is likely close to the V band.

The mentioned pulsation amplitude ratio is consistent with the relation among photometric amplitudes in different photometric bands known from previous ground-based observations, i.e. amplitude decreases with increasing wavelength (e.g. Weiss & Schneider 1984; Kurtz & Medupe 1996).

Considering the amplitude ratios for  $f_1$  between and WIRE, the expected amplitudes for  $f_4$  to  $f_6$  found by WIRE would be 0.04 to 0.12 mmag in the red filter and 0.12 to 0.40 mmag in the blue filter. Given a typical noise of  $\sim 0.06$  mmag for red and  $\sim 0.13$  mmag for blue data, we conclude that our non-detections are consistent with the WIRE results by Bruntt et al. (2009). However, the amplitude ratio for  $f_1$  may not necessarily apply for  $f_4$  and  $f_5$ , which must have a different spherical degree than  $f_1$ ,  $f_6$  and  $f_7$ , if the large frequency separation claimed by Bruntt et al. (op.cit.) is correct.

Kurtz & Balona (1984) and Bruntt et al. (2009) noticed a slight phase shift of  $\phi_V - \phi_B = -7.4 \pm 5.1^\circ$  and  $\phi_{WIRE} - \phi_B = 5.8 \pm 1.3^\circ$ . Using the pulsation phases calculated from the unbinned blue and red light curves (calculated at a fixed frequency  $f_1$ ), the observations yield a phase shift of  $\phi_R - \phi_B = 10.6 \pm 5.9^\circ$ , which is consistent with previous results.

## 6. Discussion

– ROTATION: Our red data (similar to a Johnson R bandpass) confirm the rotation period of 4.4790 days and the light curve characteristics of  $\alpha$  Cir determined by WIRE (similar to Johnson V),

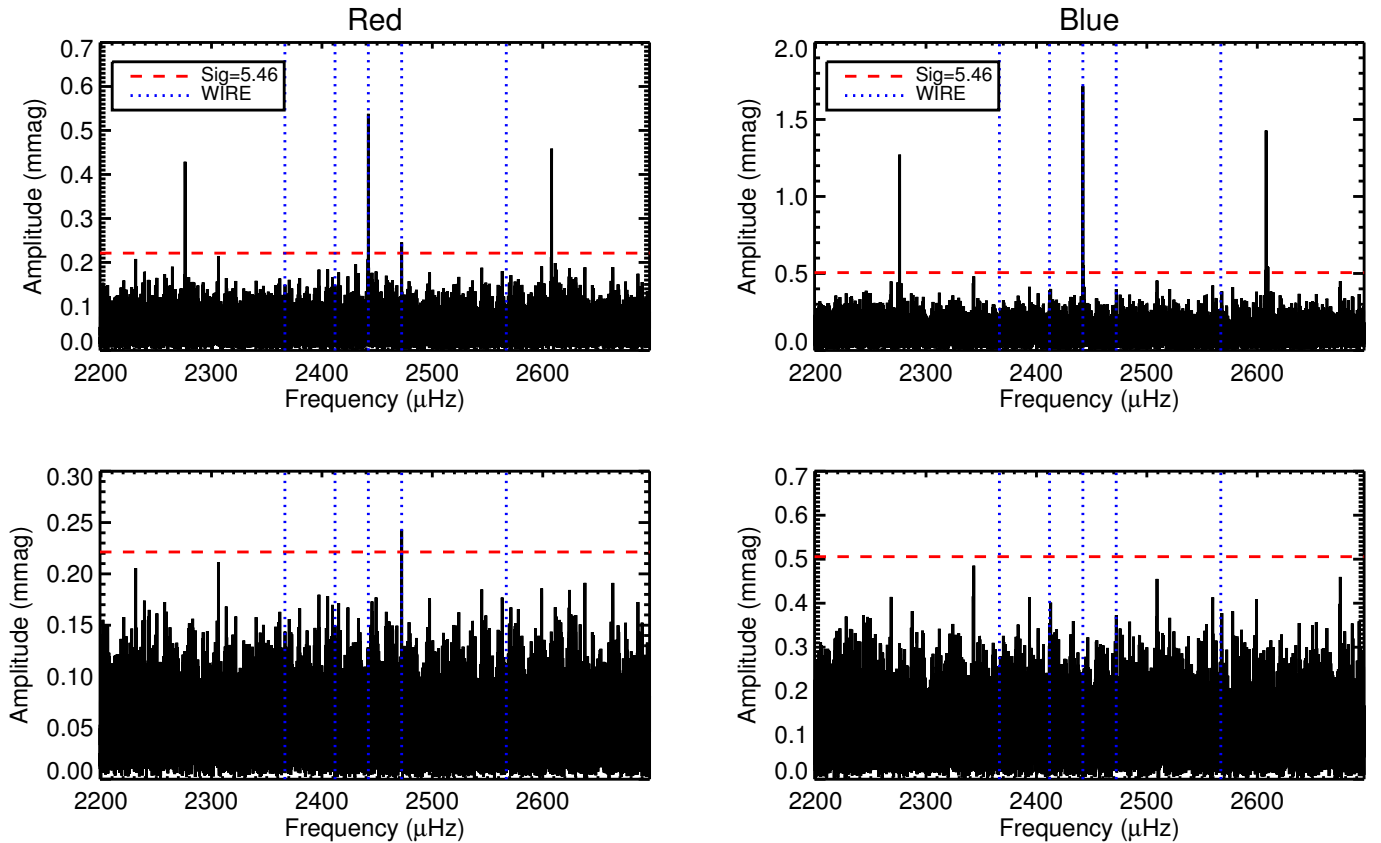


**Fig. 9.** Amplitude spectrum of the red (left panels) and blue (right panels) light curves after removing rotational variability and instrumental effects. The top panels show amplitude spectra of the data, while the bottom panels show amplitude spectra after pre-whitening of the dominant pulsation mode near  $\sim 2442 \mu\text{Hz}$ . The sidelobes seen in the top panel correspond to the orbital frequency of the satellites. Vertical dotted lines in each panel are published WIRE frequencies by Bruntt et al. (2009), while the red horizontal lines show a spectral significance corresponding to a false-alarm probability of  $10^{-5.46}$  (or  $S/N \sim 4$ ).

showing two maxima at about  $\phi = 0.2$  and  $0.8$  in our Fig. 6. This agreement is contrasted by our blue data (similar to Johnson B), which show only one maximum at about  $\phi = 0.7$ .

This profound difference in the shape of light curves obtained in different filters has not been seen before and would normally cast doubts on the reliability of our blue data. However, strong support is provided by:

- i) RV measurements which are consistent with a rotation phase plot having only one maximum (Mkrtichian & Hatzes, private communication);
- ii) magnetic field measurements, which also indicate a single-wave variation of the magnetic field (Kochukhov, private communication).

It is a known property of CP (Ap) star rotation light curves that amplitudes depend on the photometric filter used (e.g. HD 30849: Hensberge et al. (1982)). Even maxima and minima can switch (e.g. HD 53116, op.cit.) when switching colours (more examples in Schöneich, Hildebrand & Fürtig (1976)), but the disappearance of only one extremum and not also the other is unique. Other references to changes of the shape of light curves with wavelength are, e.g. Musielok et al. (1980); Kurtz & Martinez (2000); Mikulasek & Ziznovsky (2001); Mikulasek et al. (2004).

Abundance anomalies on the surfaces of magnetic CP stars, which imprint their signatures on the light curves and spectral line profiles, produce changing redistributions of stellar flux (primarily from short to longer wavelengths). This effect, which is

**Table 3.**  $\alpha$  Cir pulsation frequencies extracted from \_data

Data	Frequency ( $\mu\text{Hz}$ )	Amplitude (mmag)	Phase (0-1)	Sig
Frequency $f_1$				
red _	[ 2442.0574 ]	0.545(47)	0.191(14)	33.2
blue _	2442.0574(31)	1.72(10)	0.165(09)	63.1
WIRE	2442.0566(2)	0.652(5)		
Frequency $f_7$				
red _	2472.2401(88)	0.249(43)	0.057(32)	6.8
blue _	—	—	—	—
WIRE	2472.2272(5)	0.188(5)		

Notes: For the red \_data ( $\approx$ Johnson R), we fixed  $f_1$  to the best-fit value [in parentheses] from the blue \_data ( $\approx$ Johnson B) since the pulsation amplitude is larger in blue and has higher significance, despite the larger noise level in blue. The last column lists the spectral significance derived with SigSpec. Uncertainties are calculated via Monte Carlo simulations implemented in Period04. The reference for WIRE ( $\approx$ Johnson V) is Table 3 of Bruntt et al. (2009).

still not well understood, might lead to considerably different shapes of  $\alpha$  Cir light curves in the blue and red bands observed by BRITE-CONSTELLATION.

– Spots: Current knowledge about flux redistribution results in dark spots in short-wavelength regimes, but bright spots in the optical, if the spots are due to concentrations of elements like

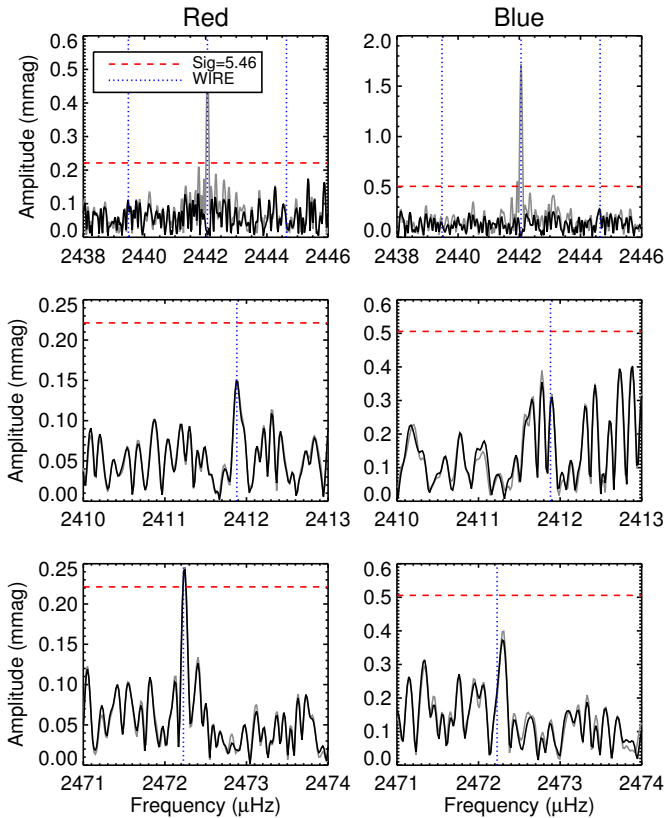


**Fig. 10.** Same as Figure 9 but for a close up of the rotational multiplet around  $f_1$  (top panels) as well as  $f_6$  (middle panels) and  $f_7$  (bottom panels). Grey and black lines show the spectrum before and after pre-whitening of  $f_1$ , respectively.

Si, Cr, or Fe (Krtićka et al. 2012). Lüftinger et al. (2010b), Shulyak et al. (2010), and Krtićka et al. (2015) find that variations of HD 37776 and  $\theta$  Aurigae in the  $u$ ,  $v$ ,  $b$ , and  $y$  Strömgren bands are caused by spots dominated by Si, Cr, and/or Fe, and those of HD 37776 are dominated by He. The elements Fe and Cr are primarily responsible for the variability of  $\epsilon$  UMa (Shulyak et al. 2010).

Considering the evidence provided by our red and blue light curves, it is not surprising that the derived spot models are unusual. We speculate that the second spot has a very different chemical composition than the first spot, which results in an equilibrium of redistributed and absorbed flux for the blue filter.

Alentjev & Mkrtichian (2010) derived very preliminary spectroscopic surface maps for  $\alpha$  Cir with spots dominated by Si and Cr, and detected abundance variations of up to 2.4 dex, which support our model solution assuming bright spots.

– **PULSATION:** The dominant frequency near 6.5 min (2442  $\mu$ Hz) is clearly detected in both data sets. With a SigSpec significance of 6.8 ( $S/N > 4$ ), we find also  $f_7$  in the frequency spectrum of the red data (Fig. 10, bottom). However,  $f_7$  does not appear in our blue data, even if we lower the threshold to a false-alarm probability of 0.1% ( $S/N \sim 3$ ). According to the amplitude scaling with wavelengths, however,  $f_7$  should appear in our blue data, if it is related to the pulsation mode of  $f_1$ . We emphasise that  $f_7$  has only been detected since 2006.

The pulsation amplitude of  $f_1$  decreases from the blue to red wavelengths (see our Table 3), a trend that is well known

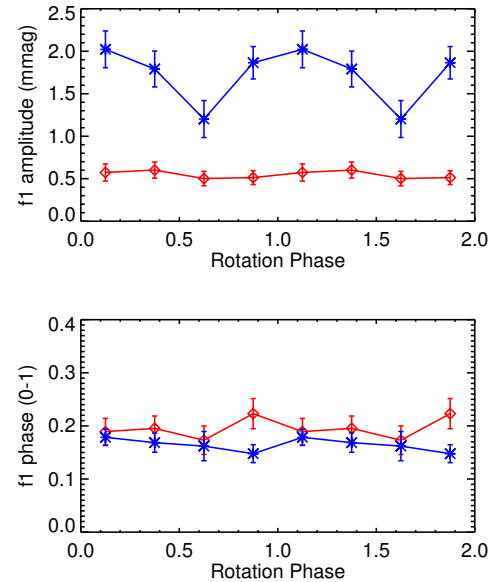


**Fig. 11.** Dependence of amplitude and phase of frequency  $f_1$  on the rotation phase of  $\alpha$  Cir, observed by blue (crosses) and red (dots)  $s$ .

for roAp stars. Since the amplitude decline rate (from Johnson B to R filters) is much steeper for pulsating late A-type stars than that of main-sequence B-type variables, Medupe & Kurtz (1998) explained the case of  $\alpha$  Cir with an outwards decreasing temperature amplitude within a narrow range ( $\sim 200$  km) of the atmosphere.

The observed phase shift between the blue and red data of  $10^\circ \pm 6^\circ$  is consistent with previous determinations. This small phase difference between red and blue light curves is in sharp contrast to considerable phase variations in the radial velocity oscillations of roAp stars, obtained from various spectral lines and at various depths of the  $H\alpha$  line (Baldry et al 1998, 1999; Ryabchikova et al. 2007). Such spectroscopic studies have shown that the pulsation properties vary significantly with atmospheric depth due to chemical stratification, leading to phase shifts between different elements.

Pulsation energy, generated below the photosphere, flows outwards into the atmosphere with changing phases. This phase variation is faster in the outer parts of the atmosphere because some of the energy leaks at the outer boundary, where the non-adiabatic damping effects are stronger. On the other hand, the phase variation is slow at the base of the atmosphere because non-adiabatic effects are weak. Hence, RV variations deduced from rare earth elements and  $H\alpha$  bisectors represent pulsation in the outer part of the atmosphere. There, non-adiabatic damping is strong, while the photometric variations primarily represent temperature effects due to pulsation near the bottom of the photosphere (optical depth  $\tau \approx 1$ ), where non-adiabatic effects are expected to be weak.

All the evidence points to high-order p-mode pulsation in  $\alpha$  Cir. We refer to Fig. 6 of Bruntt et al. (2009) where the authors discuss amplitude changes for various axisymmetric pulsation modes depending on the rotation phase of  $\alpha$  Cir. Our Fig. 11 compares amplitude and phase changes of  $f_1$  observed in the red and blue by nanosats, averaged over 25% of a full rotation cycle, respectively; our figure also addresses Fig. 10 of Kurtz et al. (1994). Our conclusion is that within the quoted errors, quadrupolar modes can be excluded for  $f_1$ , and  $\ell = 1, m = 0$  being supported.



Investigations of long-term changes of rotation and pulsation properties are obvious next research goals. Right now the time base of high quality data is too short, but observers are encouraged to monitor  $\alpha$  Cir, as BRITE-CONSTELLATION will as well.

– FINAL NOTE: High-resolution spectroscopy with high S/N, covering a full rotation cycle, is the obvious strategy to test our two bright-spot model and its dependence on wavelengths. Spectroscopy will also be critical to investigate chemical and physical spot characteristics as a function of optical depths and spectroscopy with high time resolution will be required to determine the stellar structure anomalies.

In other words, having information both on the temperature and RV variations in the atmosphere with good estimates of fundamental parameters (e.g. Bruntt et al. (2008)),  $\alpha$  Cir is one of the best roAp stars to constrain the model of pulsation in the presence of a strong magnetic field and to look deep into a star.

**Acknowledgements.** RK and WW were supported by the Austrian Science Funds (FWF) and by the Austrian Research Promotion Agency (FFG-ASAP), which also supported OK. AFJM is grateful for financial assistance from NSERC (Canada) and FRQNT (Quebec). JMM, SMR, and GAW are grateful for support from NSERC (Canada). The Polish BRITE operations are funded by the PMN grant 2011/01/M/ST9/05914. APi acknowledges the support from the NCN grant No. 2011/03/B/ST9/02667 and APo was supported by the Polish National Science Center, grant no. 2013/11/N/ST6/03051: Novel Methods of Impulsive Noise Reduction in Astronomical Images. The MCMC computations have been performed by HEF at the AIP. GH and APa received support by the Polish NCN grant 2011/01/B/ST9/05448. DH acknowledges support by the Australian Research Council's Discovery Projects funding scheme (project number DE140101364) and support by the National Aeronautics and Space Administration under Grant NNX14AB92G issued through the Kepler Participating Scientist Program. TL acknowledges funding of the Austrian FFG within ASAP11 and support by the FWF NFN projects S11601-N16 and S116 604-N16. K.Z. acknowledges support by the Austrian Fonds zur Förderung der wissenschaftlichen Forschung (FWF, project V431-NBL). Finally, the authors wish to acknowledge the spacecraft operation teams in Austria (P. Romano & M. Unterberger), Canada (Monica Chaumont, Susan Choi, Daniel Kekez, Karan Sarda, Paul Choi & Laura Bradbury) and Poland (Grzegorz Marciniśzyn & Grzegorz Woźniak), whose efforts were essential for the collection of the data used in this paper.

## References

Alentjev, D. V., Mkrtichian, D. E. 2010, *Odessa Astron. Publ.* 23, 6  
 Audard, N., Kupka, F., Morel, P., Provost, J. & Weiss, W. W. 1998, *A&A* 335, 954  
 Baglin, A., Auvergne, M., Barge, P., Deleuil, M., Catala, C., Michel, E., Weiss, W., COROT Team 2006, *ESA SP* 1306, 33  
 Baldry, I. K., Bedding, T. R., Viskum, M., Kjeldsen, H., Frandsen, S. 1998 *MNRAS* 295, 33  
 Baldry, I. K., Viskum, M., Bedding, T. R., Kjeldsen, H., Frandsen, S. 1999 *MNRAS* 302, 381  
 Balona, L. A. & Laney, C. D. 2003, *MNRAS* 344, 242  
 Bruntt H., North J. R., Cunha M., Brandão I. M., Elkin V. G., Kurtz D. W., Davis J., Bedding T. R., Jacob A. P., Owens S. M., Robertson J. G., Tango W. J., Gameiro J. F., Ireland M. J., Tuthill P. G., 2008, *MNRAS*, 386, 2039  
 Bruntt, H., Kurtz, D. W., Cunha, M. S., Brandão, I. M., Handler, G., Bedding, T. R., Medupe, T., Buzasi, D. L., Mashigo, D., Zhang, I., van Wyk, F. 2009, *MNRAS* 396, 1189  
 Dorren, J. 1987, *ApJ*, 320, 756  
 Gruberbauer, M., Saio, H., Huber, D., Kallinger, T., Weiss W. W., Guenther, D., Kuschnig, R., Matthews, J., Moffat, A., Rucinski, S., Sasselov, D. & Walker, G. 2008, *A&A*, 480, 223  
 Hensberge, H., Weiss, W. W., Catalano, F. & Schneider, H. 1982, *IBVS* 2170  
 Huber, D., Saio, H., Gruberbauer, M., Weiss, W. W., Rowe, J., Hareter, M., Kallinger, T., Reegen, P., Matthews, J., Kuschnig, R., Guenther, D., Moffat, A., Rucinski, S., Sasselov, D., & Walker, G. 2008, *A&A*, 483, 239  
 Jeffreys, H. 1961, *Theory of Probability*, 3rd ed. Oxford Univ. Press, Oxford  
 Kallinger, T., Reegen, P., & Weiss, W. W. 2008, *A&A*, 481, 571  
 Kochukhov O., Ryabchikova, T., Weiss, W. W., Landstreet, J. D. and Lyashko, D. 2007, *MNRAS* 376, 651  
 Kochukhov O., Shulyak, D. & Ryabchikova, T. 2009, *A&A* 499, 851  
 Krtićka, J., Mikulášek, Z., Henry, G. W., et al. 2009, *A&A*, 499, 567  
 Krtićka, J., Mikulášek, Z., Lüftinger, T. et al. 2012, *A&A*, 537A, 14

Krtićka, J., Mikulášek, Z., Lüftinger, T., Jagelka, M. 2015, *A&A*, 576A, 82  
 Kurtz, D. W. 1982, *MNRAS*, 200, 807  
 Kurtz, D. W., Cropper, M. S. 1981, *IBVS* 1987  
 Kurtz, D. W., Alen S., Cropper, M. S. 1981, *IBVS* 2033  
 Kurtz, D. W. & Balona, L. A. 1984, *MNRAS* 210, 779  
 Kurtz, D. W., Shibahashi, H. 1986, *MNRAS* 223, 557  
 Kurtz, D. W., Sullivan, D. J., Martinez, P., Tripe, P. 1994, *MNRAS* 270, 674  
 Kurtz, D. W. & Medupe, T. 1996, *Bull. Astron. Soc. India* 24, 291  
 Kurtz, D. W. & Martinez, P. 2000, *BaltA* 9, 253  
 Kuschnig, R., Weiss, W. W., Gruber, R., Bely, P. Y. & Jenkner, H. 1997, *A&A* 328, 544  
 Lenz, P. & Breger, M. 2005, *CoAst* 146, 53  
 Lüftinger, T., Fröhlich, H.-E., Weiss, W. W., et al. 2010a, *A&A*, 509, 43  
 Lüftinger, T., Kochukhov, O., Ryabchikova, T., Piskunov, N., Weiss, W. W., Ilyin, I. 2010b, *A&A*, 509, 71  
 Matthews, J. M., Kurtz, D. W., & Martinez, P. 1999, *ApJ*, 511, 422  
 Medupe, T., & Kurtz, D. W. 1998, *MNRAS* 299, 371  
 Mikulasek, Z. & Ziznovsky, J. 2001, *IBVS* 5188  
 Mikulasek, Z., Zverko, J., Ziznovsky, J. & Janik, J. 2004, *IAUS* 224, 657  
 Musielok, B., Lange, D., Schöneich, W., Hildebrandt, G., Zelwanowa, E., & Hempelmann, A. 1980, *AN* 301, 71  
 Orleanski, P., Graczyk, R., Mirosław Rataj, R., Schwarzenberg-Czerny, A., Zawistowski, T., Zee, R. E. 2010, *Proc. SPIE* 7745  
 Popowicz, A. et al. 2015, *in preparation*  
 Press, W. H., Teukolsky, S. A., Vetterling, W. T., & Flannery, B. P. 2007, *Numerical Recipes*, 3rd Edition (Cambridge Univ. Press, Cambridge)  
 Reegen, P. 2007, *A&A*, 467, 1353  
 Reegen, P. 2011, *CoAst* 163  
 Rosner, B. 1983 *Technometrics* 25, 165  
 Ryabchikova, T., Sachkov, M., Kochukhov O. and Lyashko, D. 2007, *A&A* 473, 907  
 Schneider, H. & Weiss, W. W. 1983, *IBVS* 2306  
 Schneider, H. & Weiss, W. W. 1989, *A&A* 210, 147  
 Schöneich, W., Hildebrand, G. & Fürtig, W. 1976, *AN* 297, 39  
 Shulyak, D., Krtićka, J., Mikulášek, Z., et al. 2010, *A&A*, 524, A66  
 Walker, G., Matthews, J., Kuschnig, R., et al. 2003, *PASP* 115, 1023  
 Walker, G., Matthews, J., Kuschnig, R., et al. 2003, *PASP* 115, 1023  
 Wayman, P. A. 1962, *Roy. Obs. Bull. Greenwich* 50  
 Weiss, W. W., Schneider, H. 1984, *A&A* 135, 148  
 Weiss, W. W., Rucinski, S. M., Moffat, A. F. J., Schwarzenberg-Czerny, A., Koudelka, O. F., Grant, C. C., Zee, R. E., Kuschnig, R., Mochnacki, St., Matthews, J. M., Orleanski, P., Pamyatnykh, A., Pigulski, A., Alves, J., Guedel, M., Handler, G., Wade, G. A., Zwintz, K. 2014, *PASP* 126, 573